Structure of a Cell Entry Defective Human Adenovirus Provides Insights into Precursor Proteins and Capsid Maturation : Cryo-EM structure of ts1 virion of an adenovirus

Yu, Xiaodi

2022-01-30

Yu , X , Mullen , T M , Abrishami , V , Huiskonen , J T , Nemerow , G R & Reddy , V S 2022 , ' Structure of a Cell Entry Defective Human Adenovirus Provides Insights into Precursor Proteins and Capsid Maturation : Cryo-EM structure of ts1 virion of an adenovirus ' , Journal of Molecular Biology , vol. 434 , no. 2 , 167350 . https://doi.org/10.1016/j.jmb.2021.167350

http://hdl.handle.net/10138/350862
https://doi.org/10.1016/j.jmb.2021.167350

Structure of a cell entry defective human adenovirus provides insights into precursor proteins and capsid maturation

Xiaodi Yu[1§], Tina-Marie Mullen[2], Vahid Abrishami[3], Juha T. Huiskonen[3], Glen R. Nemerow[2] and Vijay S. Reddy[1*]

[1]Department of Integrative Structural and Computational Biology, [2]Department of Immunology and Microbial Science, The Scripps Research Institute, La Jolla, CA 92037, USA
[3]Institute of Biotechnology, Helsinki Institute of Life Science HiLIFE, University of Helsinki, 00014, Helsinki, Finland

[§]Current address: SMPS, Janssen Research and Development, Spring House, PA 19044, USA

*Corresponding author:
Vijay S. Reddy, E-mail: reddyv@scripps.edu

Significance

Adenoviruses are initially assembled as non-infectious particles that undergo proteolytic maturation to produce infectious virions. Here we describe the capsid structure of a cell entry defective (*ts1*) mutant of a human adenovirus that provides the near-atomic resolution details of the structures and organization of precursors of minor proteins that decorate the capsid interior. Significantly, we were able to trace parts of a membrane lytic pre-protein of VI (pVI) that are sequestered deep in the hexon cavities, suggesting a likely co-assembly of pVI with hexons. Our findings are consistent with a model, where the competition between the early cleaved fragments comprising residues 1-33 and uncleaved pVI in binding to hexons, leading to reorganization of pVI molecules, their subsequent processing and release.

Abstract

Maturation of adenoviruses is distinguished by proteolytic processing of several interior minor capsid proteins and core proteins by the adenoviral protease and subsequent reorganization of adenovirus core. We report the results derived from the icosahedrally averaged cryo-EM structure of a cell entry defective form of adenovirus, designated *ts1*, at a resolution of 3.7Å as well as of the localized reconstructions of unique hexons and penton base. The virion structure revealed the structures and organization of precursors of minor capsid proteins, pIIIa, pVI and pVIII, which are closely associated with the hexons on the capsid interior. In addition to a well-ordered helical domain (a.a. 310-397) of pIIIa, highlights of the structure include the precursors of VIII display significantly different structures near the cleavage sites. Moreover, we traced residues 4-96 of the membrane lytic protein (pVI) that includes an amphipathic helix occluded deep in the hexon cavity suggesting the possibility of co-assembly of hexons with the precursors of VI. In addition, we observe a second copy of pVI ordered up to residue L40 in the peripentonal hexons and a few fragments of density corresponding to 2^{nd} and 3^{rd} copies of pVI in other hexons. However, we see no evidence of precursors of VII binding in the hexon cavity. These findings suggest the possibility that differently bound pVI molecules undergo processing at the N-terminal cleavage sites at varying efficiencies, subsequently creating competition between the cleaved and

uncleaved forms of VI, followed by reorganization, processing, and release of VI molecules from the hexon cavities.

Introduction

Adenoviruses (AdV) undergo capsid maturation that requires the proteolytic processing of minor capsid proteins (mCPs) located on the particle interior by the packaged adenoviral protease (AVP) [1-4]. This process is essential for producing the infectious virions. Previous sub-nanometer (~9.0Å) resolution cryo-EM structures of the immature form of adenovirus, represented by a temperature sensitive (*ts1*) mutant [5, 6] have shown that unlike many dsDNA viruses and bacteriophages [7, 8], adenoviruses do not undergo large-scale conformational changes. The maturation defect of the *ts1* mutant is caused by the deficiency in packaging of AVP into AdV virions, due to a point mutation (P137L) in the protease (AVP) [9]. Furthermore, although the *ts1* virions go through receptor-mediated entry into cells, they are unable to escape early endosomes and recycled back to the membrane or targeted for degradation in lysosomes [10, 11].

In this report we describe the organization of the precursor minor capsid proteins in the *ts1* virion in atomic detail and in comparison, to their mature counterparts. The *ts1* virion used in this study (termed Ad5F35-*ts1* or simply Ad5-*ts1*) comprises a shorter fiber of HAdV-B35 fiber, in place of long, native Ad5 fiber [12]. The overall structure and organization of the outer capsid proteins (hexon, penton base, fiber as well as IX) in the *ts1* virion, which do not undergo proteolytic processing during the maturation, remain the same compared to the mature human adenovirus 5 (HAdV5) structure (Fig. 1, Figs. S1, S2). In particular, we were able to assign previously established a.a. sequence of pVI residues 4-96, positioned within the hexon cavity, extending beyond the maturation cleavage site between a.a. residues 33 and 34 that includes a portion of an

amphipathic α-helix positioned deep in the hexon cavity. Furthermore, we describe the similarities and differences between the structures and interactions of the precursors of other minor capsid proteins and their counterparts in the mature AdV.

Results:

Hypervariable regions of the hexon are better ordered in the *ts1* virion

The overall structure of the most abundant major capsid protein (MCP), hexon, is mostly conserved compared to its mature counterpart (PDB:6b1t, Fig. S1A, B) [13]. However, some of the disordered residues in the hypervariable regions (HVR) in the mature virion structure (e.g., 254-257 of HVR4, 274-278 of HVR5, and 434-436 of HVR7) are ordered in the *ts1* structure, except for the HVR1, where the residues 141-159 are disordered (Table S1). The hexon structures are nearly identical (r.m.s.d: ~0.7Å) in the immature (*ts1*) and mature virions.

Of particular importance, each hexon cavity contains at least 1-2 copies of pVI molecules. Even though the density for the pVI molecules is variable in different hexons, we were able to trace residues 4-96 of one of the pVI molecules that contains a deeply occluded α-helix comprising residues 63-75 (see below). As previously observed, in addition to direct interactions between the jelly roll β (JRβ)-barrels of hexon subunits, the contiguous hexon shell is stabilized by the interactions involving the minor proteins IX on the capsid exterior, and the precursors of proteins IIIa and VIII on the capsid interior (see below) [13-17].

Penton base and fiber interactions are conserved

The structure of penton base (PB) in the *ts1* particle is also very similar to that of mature Ad5 (6b1t) with r.m.s.d of ~0.7Å for 442 aligned C-alpha atoms (Fig. S1C). As in the mature

virion, residues 35-571 are ordered with the exception of the integrin binding RGD containing loop [18, 19] comprising a.a. 303-373, which are disordered. We observe density, at lower contour levels, corresponding to multiple β-spiral repeats of the fiber (data not shown). However, we did not build any atomic models as the above density is diffused due to imposition of 5-fold symmetry on the 3-fold symmetric trimeric fiber. Also as observed in the previous structures, the density corresponding to the N-terminal "tails" of fibers is positioned in the groove formed between the two adjacent PB subunits, involving residues 189-199; 492-499 of one subunit and 217-232 from adjacent subunit [20, 21]. Of note, in addition to highly conserved N-terminal "tail" residues (a.a. 8-17) of the fiber, the residues (a.a. 27-71) that include the first β-spiral repeat, which directly contact the trough formed by PB are also well conserved among different adenoviruses.

In addition to the tight interactions between the JRβ-barrel of PB and the double JRβ-barrel of one of the peripentonal hexon (PPH) subunits (B) (Fig. S1D), the visible N-terminal (NT) residues, a.a. 35-50 of PB interact with the 109-123 of IIIa and 104-112 of a 5-fold related IIIa subunit. These interactions are analogous to those observed in the mature virion [13, 14, 20].

Protein IX (IX) interaction network is unchanged

The structure and organization of IX molecules in *ts1* virion are also essentially the same as in the mature virion (Fig. S2). Significantly, however, we built models for two complete molecules of IX, one (IX-Q) that forms a parallel helix in the 4-helical bundle (4-HLXB) sub-structure and another (IX-P) that contributes an anti-parallel helix – albeit the linker region (a.a. 62-72) of IX-P was traced in weak density. Of note, the linker regions connecting the triskelion and coiled-coil forming structures are disordered in all the 4 structurally distinct IX-molecules in the high-resolution structure of Ad5 mature virion [13]. Although the linker region of IX-Q

exhibits a helical structure (rope helix), it adopts mostly extended conformation in IX-P that forms an anti-parallel helix in the 4-HLXB (Fig. S2). As observed in the structures of mature virions, while the residues 1-57 form triskelion structures, the residues 88-140 form the coiled-coil structures [14, 22-24]. It is noteworthy that the molecules of the exterior cement protein IX does not undergo any proteolytic processing by the AVP.

An additional helical domain in precursor of IIIa (pIIIa) stabilize the vertex region

In addition to the ordered residues (a.a. 6-276) of IIIa as observed in the mature virion that form NTD and MDLD domains, an extra helical domain composed of a.a. 310-397, is found to be well ordered in the *ts1* virion (Fig. 2). This well-ordered domain, designated appendage domain (APD), which was first observed in the low resolution *ts1* structure and referred to as "molecular stitch" [5]. Although the APD was also seen in the HAdV-D26 (Ad26) structure [20], it was not as well ordered as in the *ts1* structure reported here. However, no such extra domain was visible in Ad5-WT structure (Fig. 3) [13]. The APD partly overlays on the VIII (U) molecule that interacts with the PPH and stabilizes the 3-fold junction formed at the interface of two adjacent group of nine hexons (GONs) and a PPH (hexon-1) (Fig. 2). Even though the connection between the middle (MDLD) domain (VIII interacting domain) and the appendage (APD) domains of IIIa is disordered, we observe a weakly ordered tube of density in the *ts1* structure, close to a.a. 163-173 of VIII (U), with no clear connections to either pIIIa or pVIII. Hence, we built a poly-alanine model in this density and left it as unassigned (Fig. 2A). Furthermore, as opposed to what was implied in the Ad26 structure [20], we have revised the orientation of the appendage domain relative to the middle domain within the IIIa structure, by choosing the 5-fold symmetry related APD domain likely to be connected to the MDLD domain (Fig. 2). In the revised arrangement,

143 the distance between the visible C-terminus of the MDLD and N-terminus of the APD domains is
144 closer (34 Å) in comparison to previous arrangement (59 Å). Such repositioning of APD is
145 consistent with the observation that IIIa overlays on the VIII-U molecule interacting with the
146 hexons, further fortifying the interactions between the GON-facets and PPHs. In summary, except
147 for the extra ordered regions (310-397) and minor deviation in the helix (a.a. 252-284), the rest of
148 the structure of precursor of IIIa is very similar to IIIa in the mature virions (Fig. 2B). Even though
149 the short helix (a.a. 288-301) at the of the long helix (a.a. 252-284) as observed in the mature virion
150 is missing in the *ts1* structure (Fig. 2B), an island of (3.5 turn) helical density is observed that
151 partially overlaps with the residues 296-301 of mature IIIa. We were able to build 16 a.a. poly-
152 alanine model into the density (not shown) but refrained from assigning any specific sequence to
153 it in the absence of additional information. Interestingly, the directionality of this unidentified helix
154 appears to be opposite of the helix composed of residues 288-301 in the mature virion.

155 Similar to the interactions involving IIIa in the mature virion, a.a. residues 6-104 of NTD
156 closely interact with the base of PPH as well as the residues 35-62 of IIIa protein interact closely
157 with 85-140 of neighboring (5-fold related) IIIa subunit. Five sets of these interactions stabilize
158 the PPH-PPH interactions at the vertex region. In addition, as in the mature virion, the interactions
159 between the NT of PB and IIIa (described in the section on PB and fiber) glue the pentameric
160 penton with the surrounding PPHs that forms the so called Group of Six (GOS) substructure [14].
161

162 **Structural differences in the precursors of protein VIII (pVIII) occur near the cleavage sites**

163 Two copies of pVIII are found on the capsid interior at the same locations as their
164 counterparts in the mature virion [14, 16, 20, 25, 26]. However, the major differences between the
165 mature and immature forms of VIII occur involving residues 64-173 that includes the two protease

166 cleavage sites at positions 111 and 157. Even though, the residues (64-126) comprising the first
167 cleavage site at 111 are disordered in the VIII precursor(s), the region that contains the second
168 cleavage site at 157 is ordered (Fig. 4A). Of the cleaved residues (112-157) of VIII that are released
169 from the mature form of HAdV5, the residues 127-157 are ordered in the *ts1* structure (shown in
170 purple, Fig. 4A). Furthermore, the residues 164-173 adopt helical conformation in pVIII, while
171 these residues form a β-strand structure in the mature VIII (Fig. 4B). The rest of the ordered
172 residues 1-64 and 174-227 adopt similar conformations in both precursor and mature forms.
173 Although, the structures of two distinct copies of the pVIII are nearly identical, there is an extra
174 segment of well-ordered density closely associated with the second copy of VIII (V) that is located
175 in the groove formed by the residues 18-24, 53-64 and 191-211. Based on its proximity, we
176 assigned the sequence of the VIII residues 70-88 to this density (Fig. 4A). It is noteworthy that this
177 segment is not involved in any VIII-associated cementing interactions of hexons. Furthermore, no
178 significant changes exist in the calculated buried surface areas between the pVIII (U) and the
179 contacting hexons (1, 2, and 4) (4976 $Å^2$) compared to that of the mature form of VIII (U) (5021
180 $Å^2$).
181
182 **Precursors of VI display variable conformations in the hexon cavity**
183 The precursors of VI (pVI) are found buried deep inside the cavity of the hexon trimer.
184 Each of the 4 unique hexons contains at least one molecule of pVI (pVI-type1), comprising ordered
185 residues (4-41; 57-96) in its hexon cavity (Fig. 5A, B). The best ordered molecule of pVI-type1 is
186 seen in the hexon-1 (PPH). The polarity of the chain agrees with what has been recently suggested
187 in the highest resolution cryo-EM structure of mature HAdV-C5 [13]. The continuous polypeptide
188 chain is seen till residue 41, beyond the AVP cleavage site at G33-A34. The residues 42-56, which

189 are predicted to form helical structure, are not well ordered. Significantly, however, the residues
190 63-75 form a helical structure in the upper hexon cavity, while the remaining residues 76-80 form
191 an extended chain. Interestingly, the residues 80-96, which are also suggested to form helical
192 structure, appear to from coiled structure inside the hexon cavity. The rest of the residues (97-
193 250) of pVI are disordered in all of the pVI molecules. In addition, there is a second copy of pVI
194 (pVI-type2) comprising ordered a.a. 6-40 in hexon-1 (PPH) (Fig. 5A, B). However, only a few
195 short fragments of residues (5-13, 28-34), likely corresponding to 2^{nd} or 3^{rd} copies of pVI, are
196 ordered in hexons 2-4 (Fig. 5C). It is notable that the weak density resembling a helix seen in
197 hexons 2-4, next to the well-ordered residues 65-74 in the upper cavity may correspond to the
198 disordered residues 41-56 residues, which are also known to form helix according to secondary
199 structure predictions. In other words, a.a. 41-75 are likely to form a helix-turn-helix structure in
200 the upper hexon cavity.
201
202 **Discussion**
203 The maturation and cell entry defective *ts1* mutant revealed the structures of minor capsid
204 protein precursors: pIIIa, pVI and pVIII that exhibit varying degrees of differences relative to their
205 mature counterparts. However, the overall structure and organization of the major CPs as well as
206 the exterior minor CP, IX, which do not undergo proteolytic processing by the AVP even in the
207 WT virus, are unchanged. Most of the pIIIa structure in ts1 is similar to its mature counterpart
208 except for a well-ordered helical domain (APD, a.a. 310-397) that stabilizes the hexon-hexon
209 contacts at the intersection of PPH and GON hexons on the capsid interior, thereby reinforcing the
210 vertex region. This bolstering of the vertex region is likely one of the reasons for the greater
211 thermal stability of the *ts1* particle [27, 28]. It is noteworthy that based on the difference densities
212 calculated between the *ts1* virion (current study) and the Ad5-WT particle (EMD-7034) [13], the

density corresponding to the APD domain of IIIa is clearly missing in the Ad5-WT structure, as well as in the reconstruction of Ad5-VII- (EMD-4424) [29] (Fig. 3). The differences between the structures of precursor and mature forms of VIII mainly occur near the protease cleavage sites at residues 111 and 157, while the N-terminal (1-64) and C-terminal (173-227) regions of VIII adopt structures very similar to those in the mature virion. Despite these differences between the structures of precursor and mature forms of VIII, they appear to occupy similar positions in the virion structure. Therefore, it is very likely that the changes in the cementing interactions involving pVIII upon maturation will be minor.

A striking feature seen in *ts1* structure is the organization of pVIs inserted deep within the hexon cavities, a situation that has implications in promoting hexon assembly as well as preventing premature host cell membrane lysis. While only one copy of pVI ordered up to residue 96 (pVI-type1) in each of the hexons 1-4, the 2nd and 3rd copies are ordered variably. The helix forming residues 63-75 are located deep within the hexon cavity, in agreement with the recent observations from the cryo-EM structure of VII- mutant of an AdV [29]. This kind of deep penetration of pVI into hexon cavity suggests the possibility of co-assembly of trimeric hexon and pVI together, as it would be clearly difficult to accomplish post hexon trimer formation. However, we see clear density for only one such pVI molecule in our cryo-EM maps, suggesting that the remaining copies of pVI could adopt different/random conformations, which is likely the reason for not being ordered at high resolution. Of note, although the residues 34-239 are functionally important for the membrane lysis, all or some of the N-terminal peptide (pVIn) forming residues 1-33 are critical for pVI binding to hexons [30, 31].

Beyond the densities corresponding to pVI, we did not observe any densities attributable to histone-like protein pVII in the hexon cavities, which are known to contain several helices according to secondary structure predictions. With only sequence identity of 22% with pVI,

whether or not pVII competes with pVI in binding to hexons as has been suggested by Hernando-Perez et al [29] needs to be resolved by future studies. It is possible that the difference densities attributed to VII molecules in the hexon cavities may correspond to VI molecules binding at different locations in Ad5-WT virion compared to Ad5-VII- mutant (see Fig. 3). Furthermore, there is also no equivalent density for the majority of 20 residues of protein-V reported in the HAdV-F41 structure [32], except that the residues 170-175 partially overlap with the unidentified density located between the hexon-2 and hexon-4 as seen in HAdV-26 structure [20].

Given the arrangement that one of the pVI molecules situated deep in the hexon cavity and the AVP is too big to enter and reach the sequestered cleavage sites in the hexon cavity, a question to be answered is how does this highly sequestered pVI molecule end up processed by the AVP? Even though there are 3 potential binding sites available to bind to 3-molecules of pVI, it appears that only one molecule of pVI would penetrate deep into the hexon cavity. Based on steric considerations, it is possible that some of the remaining VI molecules may adopt different conformations, particularly in the hexons 2-4, where the cleavage sites at both the N-terminus and C-terminus could be "AVP-accessible". The newly liberated N-termini of pVI (a.a. residues 1-33) can then compete for binding and dislodge the intact pVI sequestered inside the hexon cavity. These randomly oriented pVI molecules are disordered at high-resolution even in the individual localized reconstructions of the hexons 1-4 (see Methods). However, the strong densities seen connecting the hexons to the AdV core in the ~10Å resolution *ts1* structures [5, 6] may likely belong to the randomly oriented pVI molecules exposed outside the hexon cavities and accessible to AVP, which supports the above hypothesis. Furthermore, according to the observations reported here, there are 240 molecules of pVI-type1 molecules found, one each in 240 copies of hexon trimers present in the AdV capsid and another 60 of pVI-type2 molecules are likely sequestered in

PPHs. Moreover, it is possible that there could be another 60-180 copies of VI could potentially be binding to corresponding copies of hexons 2-4, amounting to a total of 360-480 molecules of VI present an HAdV virion. The lower limit of these numbers agrees with the estimates (359±24) from the mass spectrometry-based proteomics analysis [33].

Based on the *in vitro* biochemical and mass spectrometry HDX studies, it has been demonstrated that the processed pVIn (a.a. 1-33) peptides can be released from the hexons purified from the mature virions [30]. In addition, this study also indicated that the synthesized pVIn peptides, which are analogous to the cleaved pVIn fragments, can "rebind" to hexons [30]. Such reversible binding of pVIn in the hexon cavity could potentially create competition between the cleaved pVIn fragments and uncleaved (precursor) forms of pVI, resulting the "domino effect" of dislodging and/or rearrangement of pVIs bound deep in the hexon cavity. In conjunction, it is also possible that the exposure of N-terminal cleavage site at a.a. 33-34 of pVI out of the hexon cavity could occur due to "pulling forces" while accessing the C-terminal cleavage site at a.a. 239-240 and subsequent proteolysis by the AVP. It is noteworthy that the efficiency/access of AVP in Ad5-VII- mutant could be impacted by the absence of hundreds of VII molecules that play critical role in condensing and organization of dsDNA core, on which AVP is known to "slide" [34, 35]. These dislodged pVI molecules eventually become susceptible to proteolytic processing by the AVP and become available for the lysis of membranes after particle disassembly. Thus, cryo-EM of *ts1* particle revealed the structures and organization of the precursor forms of minor proteins on the capsid interior and provided new insights into potential role of pVI in the assembly of hexon trimers. Importantly, the *ts1* structure extends our knowledge of pVI processing by AVP upon virion assembly and illustrates how the trimeric hexon cavity serves as a molecular shelter for pVI, thereby protecting cells from premature lysis.

Methods:

Virus sample preparation:

The Ad5F35-*ts1* recombinant, for all practical purposes, is an Ad5 (HAdV-C5) virus with the exception that it displays a shorter fiber from Ad35 virus and carries the required mutation of a *ts1* virus, P137L in the AVP. This short fibered HAdV mutant was originally created for crystallization purposes [12, 36]. We produced a high-titered stock of replication-competent Ad5F35-*ts1* by propagation in 293β5 cells at the permissive temperature (33°C). These infectious virions were then used to infect cells in cell factories (Nunc) at an MOI of 1000 at the non-permissive temperature of 38.5°C. In our preliminary studies we found that this temperature is sufficiently high to maintain biochemical and functional characteristics of the *ts1* phenotype, while still permitting adequate host cell viability and virus production. Ad5F35-*ts1* particles were then isolated from the infected cells using standard CsCl density gradient ultracentrifugation, done twice, and followed by dialysis against the stabilization buffer (40mM Tris pH 8.1, 350mM NaCl, 5%$CaCl_2$, 10% glycerol, 10% ethylene glycol, 2% sucrose and 1% mannitol) for long time storage (1-2 weeks). The characteristics of the *ts1* phenotype were verified by the presence of unprocessed precursor capsid proteins including pVI and pVII on SDS-PAGE gels (Fig. S4) and by determining (lack of) infectivity as measured by reduction in GFP (transgene) expression (data not shown).

Cryo-EM data collection, image processing and 3D-reconstruction:

Ad5F35-*ts1* sample was dialyzed into glycerol/ethylene glycol free buffer (40mM Tris pH 8.1, 300mM NaCl and 10mM $CaCl_2$) prior to vitrification. Three microliters of the sample applied 2-3 times (with blotting in between) to 1.2/1.3 C-flat grids (Protochips) that have been plasma-

cleaned for 6s at 20mA using a Gatan Solarus cleaning system. Thereafter, the grids were plunge-frozen in liquid ethane using a Gatan Cryoplunge 3 (CP3) system and a blotting time of 3.0 s. The frozen grids were loaded into an FEI Titan Krios electron microscope operating at 300kV equipped with a Gatan K2 Summit detector. Automatic data collection was carried out using the Leginon program [37] controlling both the FEI Titan Krios (used in microprobe mode at a nominal magnification of x 22,500) and the Gatan K2 Summit camera operated in "counting mode" (pixel size = 1.31 Å). A total of 1510 movies were collected with a total exposure of 7.6 s (38 frames/image) with an exposure rate of 12 e-/pix/sec. The images were collected with defocus values ranging from -0.8µm to -3.0µm.

The movies were corrected for induced motion using the unblur program [38-40], in cisTEM [41] and followed by the estimation of contrast transfer function (CTF) parameters of each micrograph using CTFfind [42]. The CTF corrected images were used to identity 21320 particles in the "ab-initio" mode (in cisTEM) with radius and threshold values of 400 Å and 1.2, respectively. The particles were extracted into a box size of 928 X 928 pixels with a pixel size of 1.31 Å and subjected to 20 cycles of 2D classification. We selected 11,277 particles from 18 classes (Fig. S5). Then these particles were subjected to 3D refinement using an initial model derived from the atomic coordinates of Ad5 cryo-EM structure (PDB-ID: 3IYN) [14] containing only the major capsid proteins, hexons and penton base. Majority (99%) of the (11,156) particles grouped into one class at a resolution of 3.87 Å. This class of particles were subjected to a few more cycles of 3D-refinement by applying inner and outer spherical mask with radii of 300 Å and 510 Å respectively that resulted in a map of 3.72Å resolution (Fig. S6A). The final map was sharpened by applying a B-factor of -90 $Å^2$ for the data between the resolutions 8Å and 3.72Å. The data and 3D-reconstruction statistics are shown in Table S2.

Localized reconstructions of individual sub-particles:

We performed the localized reconstructions (LR) of unique hexons (hexon-1 to 4), PB-fiber (penton) complex and pIIIa subunits using Scipion package [43] that includes RELION [44] within and employing the methods that were described recently [45]. Briefly, the localized reconstructions for each of the unique capsomeres were generated by extracting the corresponding areas from the original particle images and without imposing any symmetry as described previously [20, 46]. However, the final reconstructions of the selected classes were done in cisTEM [41]. The parameters and statistics of LRs are provided in Table S3.

Model building and refinement:

The models of individual capsid proteins (e.g., hexon-1 to 4, PB, mCPs) of *ts1* virion were built into the density maps from localized reconstructions, by first docking the models of the corresponding mature counterparts from Human adenovirus 5 model (PDB-ID: 3IYN) in Chimera [47, 48] and adjusting them in Coot [49]. This followed by real space refinement in Phenix [50, 51]. Particularly, the models of inner mCPs (minor capsid proteins) required a lot of adjustments and rebuilding in Coot. Resolving the polarity of the chain was straightforward as the polypeptide chain continued beyond the cleavage site at G33-A34 that meandered deep into the hexon cavity and in agreement with recent high-resolution structure of HAdV5 [13]. Assigning the sequence for residues (57-74) of the amphipathic helix was done based on the density in the cavity of PPH (hexon-1), where it is well ordered relative to the corresponding densities in the hexons-2 to 4. After building the models for the individual CPs, they were positioned into the whole particle map of the *ts1* virion and subjected real space refinement in Phenix [50, 51]. The plot of individual

chain map-to-model correlation coefficients were calculated using Phenix (Fig. S6B). The refinement and model statistics are shown in Table S1.

Calculation of vector difference maps:

The putative difference maps were calculated using Chimera and ChimeraX [47, 48]. Briefly, the density surrounding the icosahedral asymmetric units for *ts1* (current study; EMD-24881), Ad5-WT (EMD-7034) and Ad5-VII- (EMD-4424) were extracted using "Color Zone" tool in chimera (Fig. 3), followed by adjusting the pairs of maps being compared relative to each other using the tool "Fit in Map". Later, the map to be subtracted (map-2) was "resampled on grid" of the reference map (map-1) using "vop" commands, followed by subtracting and generating the vector difference map. The features of the vector difference map were compared with the subtracted map (map-2) to identify the missing features relative to the reference map (map-1).

Author contributions:

G.R.N. and V.S.R. designed the research. T-M.M. expressed and purified the Ad5F35-*ts1*-mutant. X.Y. performed the electron microscopy experiments, data processing and obtained the initial reconstructions. V.A. and J.T.H. assisted in obtaining the localized reconstructions. V.S.R. improved the icosahedral reconstructions, generated localized reconstructions, built, and refined the 3D-models. G.R.N. and V.S.R. wrote the manuscript. All authors were asked to comment on the manuscript.

Data availability:

The cryo-EM map and coordinates of the *ts1* particle have been deposited at EMDB and in PDB with the accession codes EMD-24881 and 7S78, respectively.

Acknowledgements:

We would like to thank Dr. Francisco Asturias for his advice on electron microscopy experiments and Dr. J.C. Ducom for installing Scipion and cisTEM packages on the HPC cluster and computational support in general. This work was supported by the NIH grant R21 AI146644 to V.S.R.

Figures

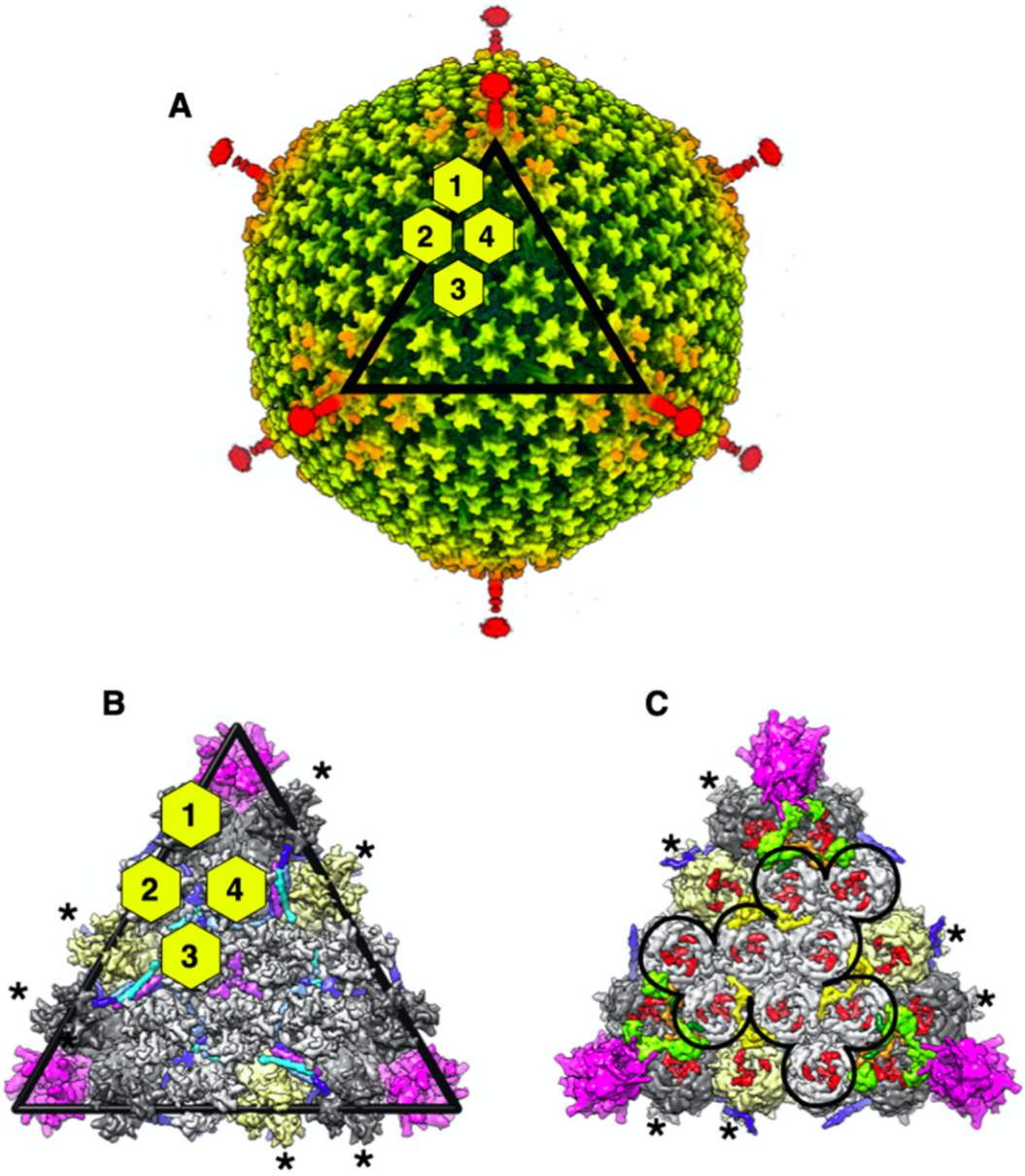

Figure 1. Overall structure and organization of *ts1*-mutant of HAdV5. **A**) Radially color-coded view, down the icosahedral 3-fold axis, of the cryo-EM reconstruction of *ts1* (Ad5F35_*ts1*) virion displaying the short fiber of Ad35. A color gradient from blue to red was used to represent the regions of the map between the radii 300Å and 500Å, respectively. The icosahedral facet is identified by the black triangle and the four structurally distinct hexon positions are distinguished

by the yellow hexagons labeled 1-4. **B**) A zoomed-in view of the icosahedral facet seen from the outside of the virion. Hexons that belong to group of nine hexons (GON) are shown in light gray, while the peripentonal hexons (PPH) are colored in dark gray. The hexons that belong to neighboring facets are identified by asterisks and/or shown in khaki color. The pentamers of penton base, located at the icosahedral vertices are shown magenta. The triskelion and 4-HLXB structures formed by the 12 protein-IX molecules - 3 copies of 4 structurally distinct IX-molecules, labeled P, Q, R and S - present in an icosahedral facet are shown in different colors blue, cyan, light blue and purple, respectively. **C)** A vertically flipped view of panel B, showing the inside view of the facet. The outline of GON structure is represented by the black line. The surface representation of ordered regions of pIIIa, pVIII-U and pVIII-V and pVI are shown, in bright green, orange, yellow and red respectively. The model fragments corresponding to islands of unassigned densities are shown as dark green surfaces. The C-terminal helix of the IX-P molecule can be seen in blue.

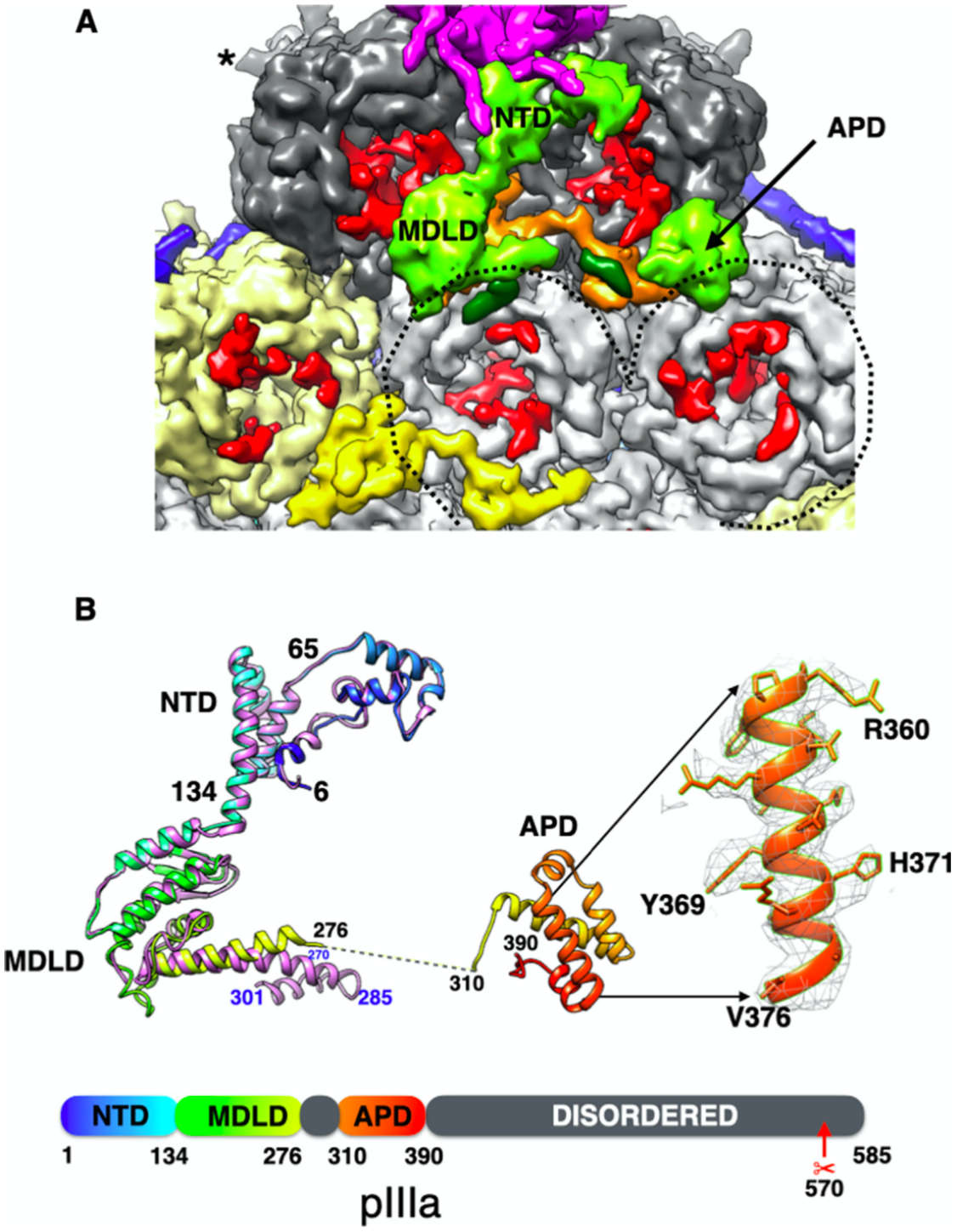

409

410 **Figure 2.** Structural comparison of precursor and mature forms of IIIa . **A)** A view from the *ts1*

411 capsid interior, underneath the vertex region, showing the location of precursor of IIIa (pIIIa),

412 depicted as bright green colored surface representation, interacting with the bases of PPH (shown

in dark gray). Hexons from the GON substructure are shown in light gray, while the hexon shown in khaki color belongs to the neighboring GON. The red colored surfaces in the hexon cavities belong to pVI and the fragments of unassigned densities are identified by dark green colored surfaces. pIIIa overlays on top of a molecule of VIII (U) shown in orange. The second VIII (V) molecule is shown in yellow color. Different domains of IIIa, NTD, MDLD and APD are labeled. The dotted line represents the GON boundary that is partially shown. **B)** Structural similarity of precursor and mature forms of IIIa from the *ts1*-mutant and mature virion structures of HAdV5 (PDB:6b1t), respectively. The ribbon diagram of pIIIa from the *ts1*-mutant structure is shown in rainbow color gradient from blue (N-terminus) to red (C-terminus), while that of the mature virion is shown in orchid color. Various domains and a few selected residues are labeled. The deviating residues in the mature IIIa are identified by blue labels. Shown on the right is representative density for an APD helix in *ts1* virion. The disordered region connecting the MDLD and APD domains is indicated as a dotted line. Shown at the bottom is the schematic diagram of pIIIa a.a. sequence that distinguishes different structural domains and the location of AVP cleavage site identified by a red colored arrow. Of note, the APD domain is disordered in the structure of mature HAdV5 virion.

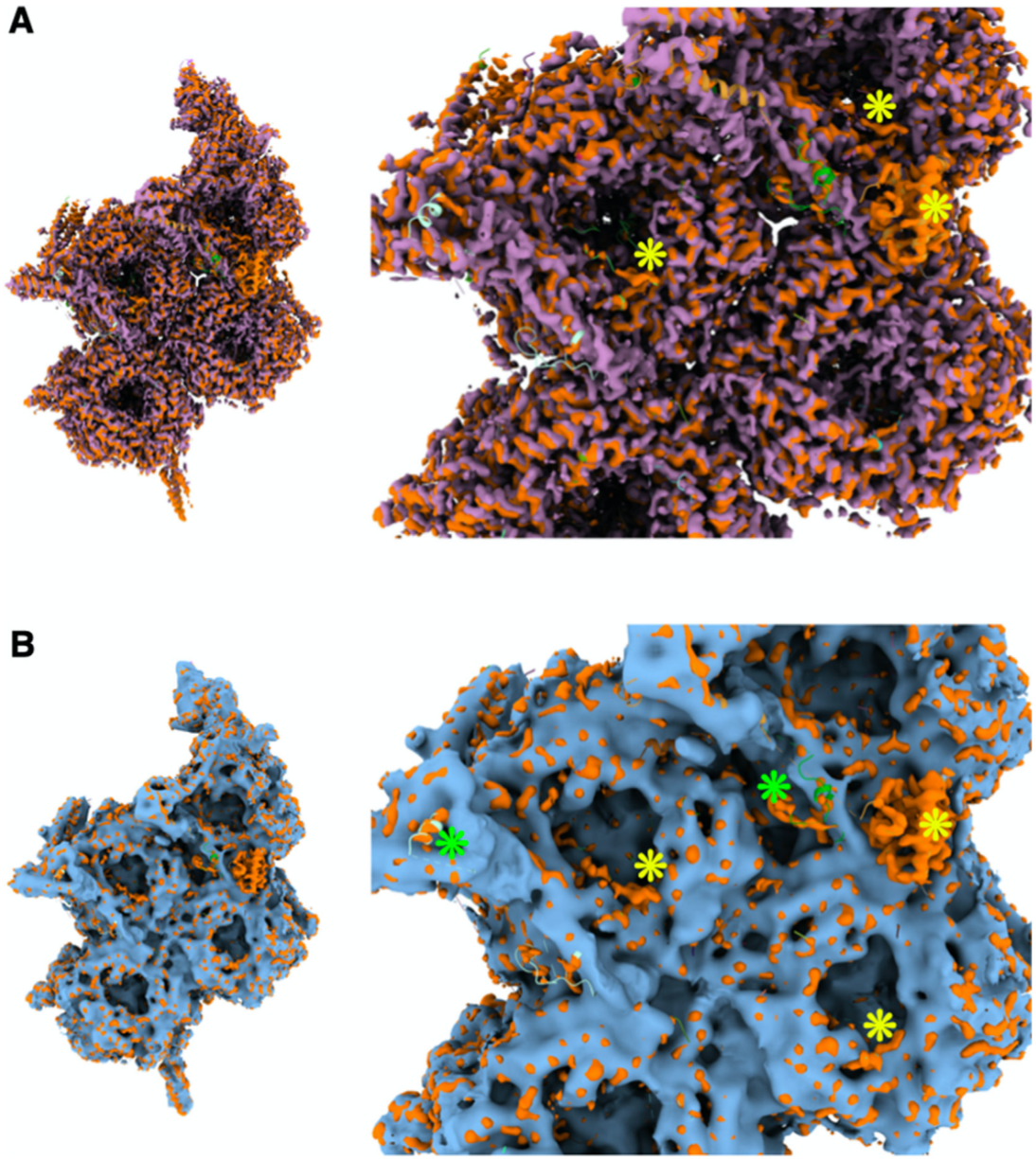

Figure 3. The vector difference densities showing the distinct features of the *ts1* virion relative to Ad-WT and Ad-VII- particles. **A)** The overlapped cryo-EM densities encompassing the icosahedral asymmetric units of *ts1* and Ad5-WT virions. The density of Ad-WT particle (EMD-7034) is shown in light purple, while that of the *ts1* virion is shown in orange. Shown on the right is a zoom-in view highlighting the absence of APD domain in Ad5-WT and a few differences in the occupancy of VI (N-termini) in the hexon cavity, identified by the yellow asterisks. Other

differences observed farther in the hexon cavity that overlap with the deeply occluded helix comprising residues 64-74 (Fig. S3). **B)** The overlapped cryo-EM densities encompassing the icosahedral asymmetric units of *ts1* virion and Ad5-VII- mutant. The density of Ad-VII- particle (EMD-4424) is shown in light blue, while that of the *ts1* virion is in orange. Shown on the right is a zoom-in view highlighting the absence of APD domain in Ad5-VII- and a few differences in the occupancy of VI (N-termini) in the hexon cavity, identified by the yellow asterisks. The green asterisks indicate the differences in VIII molecules at two distinct locations.

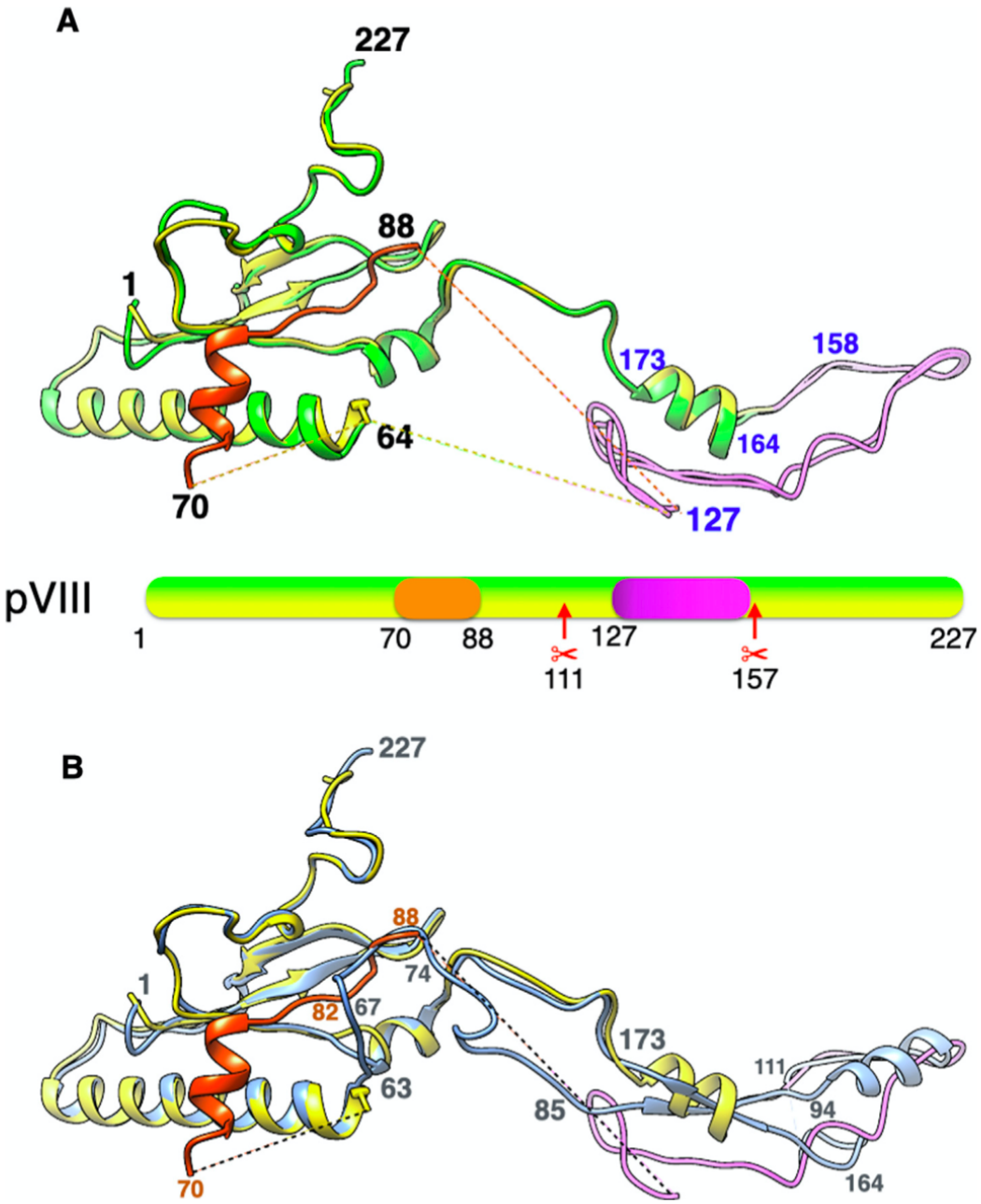

Figure 4. Structural similarities and differences between the precursor and mature forms of protein VIII. **A)** Superposition of two structurally distinct copies of pVIII found on the capsid interior of the *ts1* virion. The two copies of pVIII, termed U and V, are shown in green and yellow colors respectively. The residues between 65-126 are disordered. However, an island of density that is ordered only in pVIII-V has been assigned the sequence of residues 70-88, shown in orange. Of

the processed and released residues 112-157 in the mature form of VIII, the ordered residues 127-157 in both copies of pVIII of *ts1* are shown in purple. The disordered residues are indicated by the dashed lines. Shown at the bottom is the schematic diagram of pVIII a.a. sequence with the location of AVP cleavage sites identified by red colored arrows. **B)** Superposition of precursor and mature forms of VIII, shown in green and light blue, respectively. The amino acids are labeled according to the mature form of VIII (PDB-ID: 6b1t). The major differences between the two forms occur between residues 64-173 that includes both the cleavage sites at 111 and 157. Significantly, the residues 164-173 that form a 2-turn helix in pVIII adopt β-strand structure in the mature form.

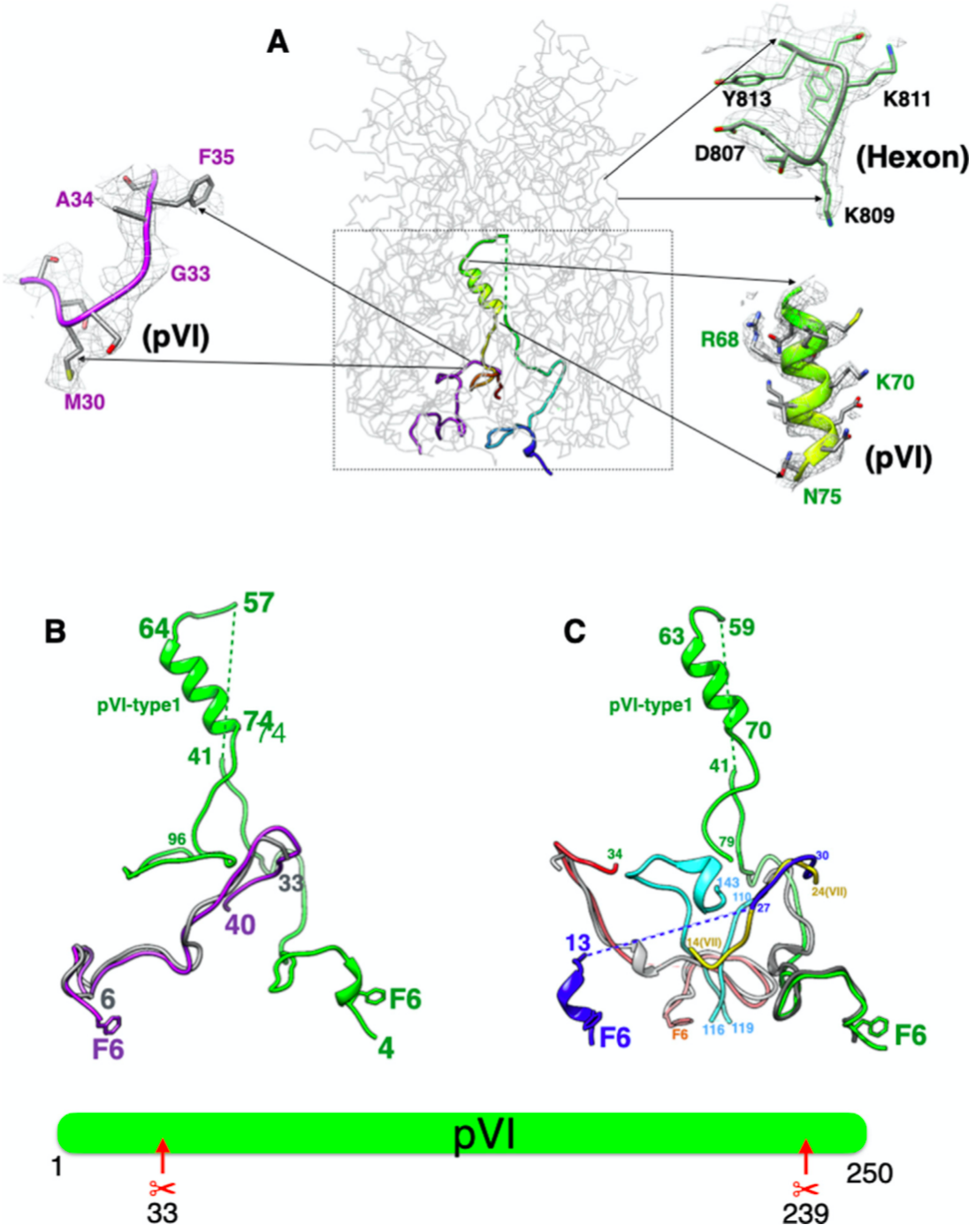

460

461 **Figure 5.** Structural comparison of precursor and mature forms of VI, residing in the hexon

462 cavities. **A)** A side view of the PPH showing the structure and locations of two copies of pVI

463 identified in the hexon cavity. Two pVI molecules are shown in ribbon representation displaying

rainbow gradient and purple colors, while the backbone trace of hexon is shown in gray. The insets show the representative densities at various structural locations of pVI and hexon. **B)** Structural comparison of precursor and mature forms of VI molecules located in the cavity of PPH (hexon-1). Two molecules of pVI found in the PPH of *ts1* virion are shown in purple and green, respectively, while the only copy of VI that is ordered in the PPH of mature HAdV5 (PDB-ID: 6b1t) is shown in gray color. The green copy of pVI is ordered till residue 96, with the missing residues 42-56 identified by the dashed line, and the purple copy is only ordered till residue 40. The remaining residues (97-250) are disordered. The ordered (6-33) copy of mature VI (gray) superimposes well on to one the partially ordered (purple) copy of pVI. **C)** Structural comparison of precursor and mature forms of VI molecules located in the cavity of hexon-2. There is one significantly ordered copy and two partially ordered copies of pVI in hexon-2 of *ts1* structure, which are shown in green, red, and blue, respectively. Residue numbers of the respective molecules are labeled in the corresponding colors. In addition to two N-terminal segments (5-33) of mature VI (shown in gray), a large segment of residues 110-143 (shown in cyan) ordered in hexon-2 of HAdV. While the N-terminal segments (5-33) of mature VI molecules superimpose well onto their counterparts in the *ts1* structure, no structures equivalent of the larger segment (110-143) is found in the *ts1*-virion. Significantly, the 11-residue peptide fragment assigned to a.a. 14-24 of VII (shown in gold) in mature Ad5, overlaps with the partially ordered copy of VI in *ts1* virion. Shown at the bottom is the schematic diagram of pVI a.a. sequence with the location of AVP cleavage sites identified by red colored arrows.

References:

[1] D'Halluin JC. Virus assembly. Curr Top Microbiol Immunol. 1995;199 (Pt 1):47-66.
[2] Weber JM. Role of endoprotease in adneovirus infection. Austin, TX: R.G. Landes; 1999.
[3] Greber UF. Virus assembly and disassembly: the adenovirus cysteine protease as a trigger factor. Rev Med Virol. 1998;8:213-22.
[4] Greber UF, Webster P, Weber J, Helenius A. The role of the adenovirus protease on virus entry into cells. EMBO J. 1996;15:1766-77.
[5] Perez-Berna AJ, Marabini R, Scheres SH, Menendez-Conejero R, Dmitriev IP, Curiel DT, et al. Structure and uncoating of immature adenovirus. J Mol Biol. 2009;392:547-57.
[6] Silvestry M, Lindert S, Smith JG, Maier O, Wiethoff CM, Nemerow GR, et al. Cryo-electron microscopy structure of adenovirus type 2 temperature-sensitive mutant 1 reveals insight into the cell entry defect. Journal of virology. 2009;83:7375-83.
[7] Steven AC, Heymann JB, Cheng N, Trus BL, Conway JF. Virus maturation: dynamics and mechanism of a stabilizing structural transition that leads to infectivity. Curr Opin Struct Biol. 2005;15:227-36.
[8] Hendrix RW, Johnson JE. Bacteriophage HK97 capsid assembly and maturation. Adv Exp Med Biol. 2012;726:351-63.
[9] Rancourt C, Keyvani-Amineh H, Sircar S, Labrecque P, Weber J. Proline 137 is critical for adenovirus protease encapsidation and activation but not enzyme activity. Virology. 1995;209:167-73.
[10] Gastaldelli M, Imelli N, Boucke K, Amstutz B, Meier O, Greber UF. Infectious adenovirus type 2 transport through early but not late endosomes. Traffic. 2008;9:2265-78.
[11] Cotten M, Weber JM. The adenovirus protease is required for virus entry into host cells. Virology. 1995;213:494-502.
[12] Smith TA, Idamakanti N, Rollence ML, Marshall-Neff J, Kim J, Mulgrew K, et al. Adenovirus serotype 5 fiber shaft influences in vivo gene transfer in mice. Hum Gene Ther. 2003;14:777-87.
[13] Dai X, Wu L, Sun R, Zhou ZH. Atomic Structures of Minor Proteins VI and VII in the Human Adenovirus. Journal of virology. 2017.
[14] Liu H, Jin L, Koh SB, Atanasov I, Schein S, Wu L, et al. Atomic structure of human adenovirus by cryo-EM reveals interactions among protein networks. Science. 2010;329:1038-43.
[15] Reddy VS, Natchiar SK, Stewart PL, Nemerow GR. Crystal structure of human adenovirus at 3.5 A resolution. Science. 2010;329:1071-5.
[16] Kundhavai Natchiar S, Venkataraman S, Mullen TM, Nemerow GR, Reddy VS. Revised Crystal Structure of Human Adenovirus Reveals the Limits on Protein IX Quasi-Equivalence and on Analyzing Large Macromolecular Complexes. J Mol Biol. 2018.
[17] Reddy VS, Barry MA. Structural Organization and Protein-Protein Interactions in Human Adenovirus Capsid. Subcell Biochem. 2021;96:503-18.
[18] Zubieta C, Schoehn G, Chroboczek J, Cusack S. The structure of the human adenovirus 2 penton. Mol Cell. 2005;17:121-35.
[19] Chiu CY, Mathias P, Nemerow GR, Stewart PL. Structure of adenovirus complexed with its internalization receptor, alphavbeta5 integrin. Journal of virology. 1999;73:6759-68.
[20] Yu X, Veesler D, Campbell MG, Barry ME, Asturias FJ, Barry MA, et al. Cryo-EM structure of human adenovirus D26 reveals the conservation of structural organization among human adenoviruses. Sci Adv. 2017;3:e1602670.

[21] Liu H, Wu L, Zhou ZH. Model of the trimeric fiber and its interactions with the pentameric penton base of human adenovirus by cryo-electron microscopy. J Mol Biol. 2011;406:764-74.
[22] Reddy VS. The Role of Hexon Protein as a Molecular Mold in Patterning the Protein IX Organization in Human Adenoviruses. J Mol Biol. 2017;429:2747-51.
[23] Matteson NL, Barry MA, Reddy VS. Structure-based assessment of protein-protein interactions and accessibility of protein IX in adenoviruses with implications for antigen display. Virology. 2018;516:102-7.
[24] Saban SD, Silvestry M, Nemerow GR, Stewart PL. Visualization of alpha-helices in a 6-angstrom resolution cryoelectron microscopy structure of adenovirus allows refinement of capsid protein assignments. Journal of virology. 2006;80:12049-59.
[25] Fabry CM, Rosa-Calatrava M, Conway JF, Zubieta C, Cusack S, Ruigrok RW, et al. A quasi-atomic model of human adenovirus type 5 capsid. EMBO J. 2005;24:1645-54. Epub 2005 Apr 21.
[26] Saban SD, Nepomuceno RR, Gritton LD, Nemerow GR, Stewart PL. CryoEM structure at 9A resolution of an adenovirus vector targeted to hematopoietic cells. J Mol Biol. 2005;349:526-37.
[27] Perez-Berna AJ, Ortega-Esteban A, Menendez-Conejero R, Winkler DC, Menendez M, Steven AC, et al. The role of capsid maturation on adenovirus priming for sequential uncoating. J Biol Chem. 2012;287:31582-95.
[28] Wiethoff CM, Wodrich H, Gerace L, Nemerow GR. Adenovirus protein VI mediates membrane disruption following capsid disassembly. Journal of virology. 2005;79:1992-2000.
[29] Hernando-Perez M, Martin-Gonzalez N, Perez-Illana M, Suomalainen M, Condezo GN, Ostapchuk P, et al. Dynamic competition for hexon binding between core protein VII and lytic protein VI promotes adenovirus maturation and entry. Proc Natl Acad Sci U S A. 2020;117:13699-707.
[30] Snijder J, Benevento M, Moyer CL, Reddy V, Nemerow GR, Heck AJ. The Cleaved N-Terminus of pVI Binds Peripentonal Hexons in Mature Adenovirus. J Mol Biol. 2014.
[31] Reddy VS, Nemerow GR. Structures and organization of adenovirus cement proteins provide insights into the role of capsid maturation in virus entry and infection. Proc Natl Acad Sci U S A. 2014;111:11715-20.
[32] Rafie K, Lenman A, Fuchs J, Rajan A, Arnberg N, Carlson LA. The structure of enteric human adenovirus 41-A leading cause of diarrhea in children. Sci Adv. 2021;7.
[33] Benevento M, Di Palma S, Snijder J, Moyer CL, Reddy VS, Nemerow GR, et al. Adenovirus Composition, Proteolysis and Disassembly Studied by in-depth Qualitative and Quantitative Proteomics. J Biol Chem. 2014.
[34] Blainey PC, Graziano V, Perez-Berna AJ, McGrath WJ, Flint SJ, San Martin C, et al. Regulation of a viral proteinase by a peptide and DNA in one-dimensional space: IV. viral proteinase slides along DNA to locate and process its substrates. J Biol Chem. 2013;288:2092-102.
[35] Graziano V, Luo G, Blainey PC, Perez-Berna AJ, McGrath WJ, Flint SJ, et al. Regulation of a viral proteinase by a peptide and DNA in one-dimensional space: II. adenovirus proteinase is activated in an unusual one-dimensional biochemical reaction. J Biol Chem. 2013;288:2068-80.
[36] Reddy VS, Natchiar SK, Gritton L, Mullen TM, Stewart PL, Nemerow GR. Crystallization and preliminary X-ray diffraction analysis of human adenovirus. Virology. 2010;402:209-14.
[37] Suloway C, Pulokas J, Fellmann D, Cheng A, Guerra F, Quispe J, et al. Automated molecular microscopy: the new Leginon system. J Struct Biol. 2005;151:41-60.

[38] Brilot AF, Chen JZ, Cheng A, Pan J, Harrison SC, Potter CS, et al. Beam-induced motion of vitrified specimen on holey carbon film. J Struct Biol. 2012;177:630-7.
[39] Campbell MG, Cheng A, Brilot AF, Moeller A, Lyumkis D, Veesler D, et al. Movies of ice-embedded particles enhance resolution in electron cryo-microscopy. Structure. 2012;20:1823-8.
[40] Grant T, Grigorieff N. Measuring the optimal exposure for single particle cryo-EM using a 2.6 A reconstruction of rotavirus VP6. Elife. 2015;4:e06980.
[41] Grant T, Rohou A, Grigorieff N. cisTEM, user-friendly software for single-particle image processing. Elife. 2018;7.
[42] Mindell JA, Grigorieff N. Accurate determination of local defocus and specimen tilt in electron microscopy. J Struct Biol. 2003;142:334-47.
[43] de la Rosa-Trevin JM, Quintana A, Del Cano L, Zaldivar A, Foche I, Gutierrez J, et al. Scipion: A software framework toward integration, reproducibility and validation in 3D electron microscopy. J Struct Biol. 2016;195:93-9.
[44] Scheres SH. RELION: implementation of a Bayesian approach to cryo-EM structure determination. J Struct Biol. 2012;180:519-30.
[45] Abrishami V, Ilca SL, Gomez-Blanco J, Rissanen I, de la Rosa-Trevin JM, Reddy VS, et al. Localized reconstruction in Scipion expedites the analysis of symmetry mismatches in cryo-EM data. Prog Biophys Mol Biol. 2021;160:43-52.
[46] Ilca SL, Kotecha A, Sun X, Poranen MM, Stuart DI, Huiskonen JT. Localized reconstruction of subunits from electron cryomicroscopy images of macromolecular complexes. Nat Commun. 2015;6:8843.
[47] Pettersen EF, Goddard TD, Huang CC, Couch GS, Greenblatt DM, Meng EC, et al. UCSF Chimera--a visualization system for exploratory research and analysis. J Comput Chem. 2004;25:1605-12.
[48] Goddard TD, Huang CC, Meng EC, Pettersen EF, Couch GS, Morris JH, et al. UCSF ChimeraX: Meeting modern challenges in visualization and analysis. Protein Sci. 2018;27:14-25.
[49] Emsley P, Lohkamp B, Scott WG, Cowtan K. Features and development of Coot. Acta crystallographica Section D, Biological crystallography. 2010;66:486-501.
[50] Adams PD, Afonine PV, Bunkoczi G, Chen VB, Davis IW, Echols N, et al. PHENIX: a comprehensive Python-based system for macromolecular structure solution. Acta crystallographica Section D, Biological crystallography. 2010;66:213-21.
[51] Afonine PV, Poon BK, Read RJ, Sobolev OV, Terwilliger TC, Urzhumtsev A, et al. Real-space refinement in PHENIX for cryo-EM and crystallography. Acta Crystallogr D Struct Biol. 2018;74:531-44.